PHYSICAL REVIEW B **87**, 085202 (2013)

Strong excitonic effects in the optical properties of graphitic carbon nitride g-C_3N_4 from first principles

Wei Wei and Timo Jacob*

Institute of Electrochemistry, Ulm University, Albert-Einstein-Allee 47, D-89081 Ulm, Germany

(Received 6 November 2012; revised manuscript received 24 January 2013; published 8 February 2013)

Graphitic carbon nitride (g-C_3N_4) has recently triggered extensive investigations due to its potential applications, such as in direct photochemical water splitting, CO_2 activation, and transition-metal-free spintronics. However, electronic, and particularly the optical properties of g-C_3N_4 still have not been well established. Based on one of the state-of-the-art approaches—many-body Green's function theory (i.e., GW + BSE)—absorption of ultraviolet light by g-C_3N_4 is found to be determined by strong *excitonic effects* with a significantly large binding energy assigned to the bound excitons. Dark states have also been found in g-C_3N_4, which can affect the photoluminescence yield of g-C_3N_4. We find that the band gap of g-C_3N_4 probably can be tuned by adjusting the condensation (dimensionality) to initiate excitonic absorption in the visible light region, which might help improve the solar energy conversion efficiency.

DOI: 10.1103/PhysRevB.87.085202 PACS number(s): 78.20.−e, 71.35.Cc, 71.15.Mb

I. INTRODUCTION

Since Liu and Cohen predicted carbon nitride (C_3N_4) to be a superhard material,[1] it has attracted considerable attention due to its promising applications in mechanical, optical, and electronic devices.[2–4] C_3N_4 can exist in several allotropes, of which graphitic C_3N_4 (g-C_3N_4),[5,6] being prepared by condensation from suitable molecular precursors,[7,8] is considered the most stable one at ambient conditions. As shown in Fig. 1, triazine and tri-s-triazine are widely deemed as the primary building blocks of g-C_3N_4 and its various derivatives, where theoretical studies showed a preference for tri-s-triazine-based structures by roughly 30 kJmol^{-1} over triazine-based systems.[9] By analogy to graphite, bulk g-C_3N_4 is a layered solid with *ABA* stacking of hexagonal planes of carbon and nitrogen atoms.[10,11] This leads to anisotropy in chemical bonding, which makes g-C_3N_4 a typical example of a quasi-two-dimensional structure with technological interests. As graphene, a single layer of carbon atoms exfoliated from graphite,[12,13] single-layered g-C_3N_4 might conceal interesting properties and many application potentials. In recent experiments, g-C_3N_4-based materials were identified as metal-free photocatalysts for both green synthetic chemistry and solar energy conversion.[6,14–20] As an effective and all-organic photocatalyst for H_2 evolution, water splitting has been realized, for instance, upon the thermally and chemically stable *polymeric* g-C_3N_4 under visible light irradiation.[14,20] Nevertheless, derivatives of g-C_3N_4, such as g-C_3N_4 networks and even the polymeric g-C_3N_4, are difficult to characterize and process due to their insolubility.[5] More important, the fundamental electronic and, in particular, the optical properties of g-C_3N_4 are far from being explicitly understood, which leads to uncertainties and limitations to its further exploration.

Recently, features of g-C_3N_4 have been illustrated. For simplicity, hereafter, we refer to g-C_3N_4 single layer constructed from triazine [Fig. 1(a)] as g-CN1, while the one constructed from tri-s-triazine [Fig. 1(b)] is referred to as g-CN2. In carbon self-doped g-CN1,[21] ferromagnetism and half metallicity were predicted from the first-principles density functional theory (DFT) studies, which highlighted a new candidate for application in transition-metal-free spintronics.[22] As for g-CN2, it was considered an ideal substrate for graphene with the formation of a well-defined electron-hole (e-h) puddle and the band gap opening in graphene.[23] In Ref. 23, based on the optical absorption spectra obtained by means of hybrid functional and independent-particle approximations, the authors declared an enhanced optical response of interfaced g-CN2/graphene in the visible light region. As we will discuss later, nevertheless, independent-particle approximations always fail in calculating the optical properties, and correct descriptions of the excited properties of g-C_3N_4 are still in need.

As in the quasi-two-dimensional hexagonal graphite and two-dimensional graphene, Coulomb interactions between excited electrons and holes, i.e., *excitonic effects*, play a pivotal role in determining the optical properties.[24–27] The excitonic effects in systems with reduced dimensionality are a consequence of two well-defined factors:[28] quantum size confinement and less efficient electronic screening. In low-dimensional systems, enhanced electron-electron (e-e) correlation gives rise to large quasiparticle (QP) band gaps. The large overlap between electron and hole wave functions due to the confinement effects leads to a reduced screening between the excited e-h and thus the formation of strongly bound excitons with considerable binding energy. The excitonic effects in structures manifesting strong anisotropic screening are of importance for corresponding applications in photocatalysts and optoelectronic devices. As a result, for an appropriate description of the electronic and optical properties of g-CNs it is highly appealing to include many-body effects, i.e., e-e correlation and e-h interaction, which are completely missing in independent-particle approximations.

Although the DFT approach has been proven to be very successful in describing the ground-state properties of a large variety of materials, it is not expected to provide a sufficient description of the properties of excited states, such as optical absorption and luminescence. Absorption of light involves two-particle properties, which are quite different from the one-electron excited properties described at the pure electronic level. Within the *ab initio* frameworks, the many-body Green's

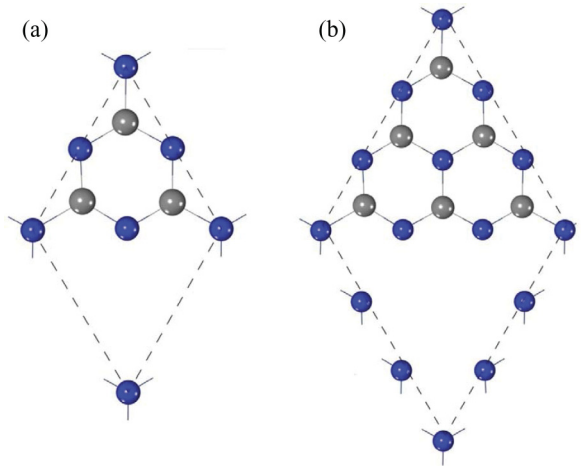

FIG. 1. (Color online) Unit cell of g-CN1 (triazine) (a) and g-CN2 (tri-s-triazine) (b). Gray and blue spheres respectively represent C and N atoms, while dashed lines indicate the lattice.

function approach is able to provide reliable results for calculating excited states.[29,30] In this regard, quantitative predictions of the absorption spectra of a wide class of systems become tractable by adopting the GW approximation and solving the Bethe-Salpeter equation (BSE).[30,31] The GW + BSE scheme, which stands for a state-of-the-art method for calculating the direct transitions, properly includes the e-e correlation and e-h interaction and thus gives results often in excellent agreement with experiments.[27,32–38]

II. METHODS

An appropriate description of the ground-state properties is essential to perform QP calculations within many-body perturbation theory. The wave functions and energies of the Kohn-Sham equations provide a good starting point for many-body calculations within the GW approximation. Therefore, we treated the electronic ground state of g-CNs using first-principles DFT with the local density approximation (LDA) for exchange and correlation as implemented in the QUANTUM ESPRESSO distribution.[39] A plane−wave basis and norm-conserving pseudopotentials for ion-electron interactions were used. The plane-wave cutoff energy was set as 50 Ry, and a Monkhorst-Pack $\mathbf{k}$ mesh of 18×18 points was adopted. A vacuum spacing of 17 Å was used to separate periodic images. The cell parameters (for bulk phase) and atomic positions were fully relaxed until an energy convergence of $5.0 \times 1\,0^{-6}$ eV and a force convergence on atoms of 0.01 eV/Å were achieved.

Starting from the LDA wave functions and Coulomb screening, we calculated the QP energies ("true" single-particle excitation energies) within the GW approximation for the electron self-energy operator Σ by solving the Dyson equation[30]

$$\left[-\frac{\nabla^2}{2} + V_{\text{ext}} + V_{\text{Hartree}} + \Sigma\left(E^{qp}_{n\mathbf{k}}\right)\right]\psi^{qp}_{n\mathbf{k}} = E^{qp}_{n\mathbf{k}}\psi^{qp}_{n\mathbf{k}}.$$

The equation was solved non-self-consistently, i.e., within the G_0W_0 approximation, leading to $\Sigma = iG_0W_0$. The DFT-LDA eigenvalues and eigenfunctions were used to construct G_0, which takes the form[40]

$$G^{n\mathbf{k}}_0(\omega) = \frac{f_{n\mathbf{k}}}{\omega - \varepsilon_{n\mathbf{k}} - i0^+} + \frac{1 - f_{n\mathbf{k}}}{\omega - \varepsilon_{n\mathbf{k}} + i0^+}$$

with $f_{n\mathbf{k}}$ being the occupation factor and $\varepsilon_{n\mathbf{k}}$ the Kohn-Sham energy. The exact Green's function is then given by the Dyson equation. The equation of motion for ε^{-1}, the inverse dielectric function, follows from that of the reducible response function χ as

$$\varepsilon^{-1}_{\mathbf{GG}'}(\mathbf{q},\omega) = \delta_{\mathbf{GG}'} + v(\mathbf{q}+\mathbf{G})\chi_{\mathbf{GG}'}(\mathbf{q},\omega).$$

The dynamical screening effects in self-energy were taken into account through the generalized plasmon pole model,[40,41] in which the ε^{-1} function is approximated with a single pole function

$$\varepsilon^{-1}_{\mathbf{GG}'}(\mathbf{q},\omega) \approx \delta_{\mathbf{GG}'} + R_{\mathbf{GG}'}(\mathbf{q})\{[\omega - \Omega_{\mathbf{GG}'}(\mathbf{q}) + i0^+]^{-1} - [\omega + \Omega_{\mathbf{GG}'}(\mathbf{q}) - i0^+]^{-1}\}.$$

The coupled excitonic effects and optical spectra were then obtained by solving the BSE in terms of the two-particle Green's function of quasielectron and quasihole states, which corresponds to the diagonalization of the following exciton equation:[30,31,40]

$$\left(E^{qp}_{c\mathbf{k}} - E^{qp}_{v\mathbf{k}}\right)A^S_{vc\mathbf{k}} + \Sigma_{\mathbf{k}'v'c'}\langle vc\mathbf{k}|K_{e-h}|v'c'\mathbf{k}'\rangle A_{v'c'\mathbf{k}'}{}^S = \Omega^S A^S_{vc\mathbf{k}},$$

where $A^S_{vc\mathbf{k}}$ are the exciton amplitudes, Ω^S are the excitation energies, and K_{e-h} is the kernel describing the screened interaction between excited electrons and holes. $\langle vc\mathbf{k}|$ and $|v'c'\mathbf{k}'\rangle$ are the quasielectron and quasihole states, respectively. The static screening in the direct term was calculated within the random-phase approximation (RPA).[42] We considered just the resonant part of the Bethe-Salpeter Hamiltonian, i.e., the Tamm-Dancoff approximation,[43] with which the non-Hermitian BSE reduces to a Hermitian one and can be solved by an efficient iterative method. Finally, the dielectric function can be expressed as[40]

$$\varepsilon_M(\omega) \equiv 1 - \lim_{\mathbf{q}\to 0}\frac{8\pi}{|\mathbf{q}|^2\Omega N_{\mathbf{q}}}\sum_{nn'\mathbf{k}}\sum_{mm'\mathbf{k}'}\rho^*_{n'n\mathbf{k}}(\mathbf{q},\mathbf{G})\rho_{m'm\mathbf{k}'}(\mathbf{q},\mathbf{G}') \times \sum_{\lambda}\frac{A^{\lambda}_{n'n\mathbf{k}}(A^{\lambda}_{m'm\mathbf{k}'})^*}{\omega - E_{\lambda}}.$$

In both GW and BSE calculations, the Coulomb interaction was truncated after 33 Å along the direction perpendicular to the plane because of its long-range nature; otherwise, unphysical interactions between periodic images lead to deviations from the physics of an isolated system.[44] The GW and BSE calculations were performed using YAMBO code.[40]

III. RESULTS AND DISCUSSION

The top of the valance band of g-CNs is mainly composed of the $2p$ orbital of N atoms, while hybridized N $2p$ and C $2p$ orbitals predominately contribute to the bottom of the conduction band. Figures 2(a) and 2(b), respectively, correspond to the band structures of g-CN1 and g-CN2 in the two-dimensional Brillouin zone. As for both g-CN1 and g-CN2, bands near the Fermi level are relatively flat indicating localized electrons, which is a consequence of the potential

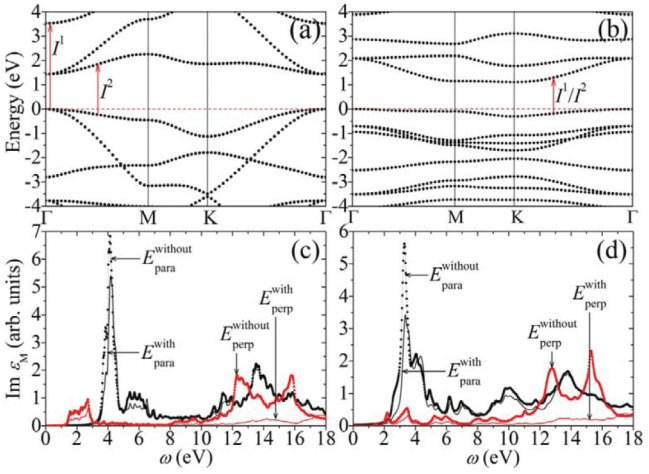

FIG. 2. (Color online) Band structure of g-CN1 (a) and g-CN2 (b) in the two-dimensional hexagonal Brillouin zone; the arrows indicate the vertical interband transitions contributing to the bound excitons I^1 and I^2, and the Fermi level was set at zero. Imaginary part of the macroscopic dielectric function ε_M for light polarization parallel (E_{para}, black lines) and perpendicular (E_{perp}, red lines) to the surface plane of g-CN1 (c) and g-CN2 (d) calculated with (solid lines) and without (dotted lines) consideratoin of LFE.

inhomogeneity within the g-CN layers. The flatness in g-CN1 is much weaker than that in g-CN2. At the DFT-LDA level, as shown in Fig. 2(a), g-CN1 demonstrates a direct band gap of 1.43 eV at the Γ point of the hexagonal Brillouin zone. The band structure of g-CN2, as shown in Fig. 2(b), demonstrates an indirect gap of 1.11 eV between the Γ and K points, and a direct gap of 2.09 eV at the Γ point. As for g-CN2, band-gap values at the DFT level are also available from previous works; for instance, Wang *et al.* obtained a value of 2.1 eV,[14] which is in good agreement with our result. However, it is well known that DFT generally underestimates band gap as the independent-electron picture breaks down because of the strong Coulomb interactions.[45,46] In order to improve the theoretical evaluation of band gap, hybrid functionals are sometimes used in DFT calculations. For example, a hybrid-DFT band gap of g-CN2 was calculated to be 2.73 eV (HSE06)[18] or 3.01 eV (B3LYP).[47]

In the present work, we use the GW approximation, which takes the concept of "QP" into account, to describe the band structures of g-CNs. After considering the e-e self-energy effects, the band gap of g-CN1 is strongly enlarged to 4.24 eV, and 5.22 (4.15) eV for the direct (indirect) gap of g-CN2. Such large QP corrections to Kohn-Sham LDA eigenvalues are a consequence of the enhanced e-e correlation due to the confinement effect. In other words, it is the screening behavior of the many-body medium that determines the QP corrections. In addition, the QP corrections manifest a complicated momentum and energy dependence, so that there is no simple "*scissor rule*" to obtain the QP band structure.[28] This behavior, which cannot be correctly described by DFT−LDA, results from the nonlocal character of the self-energy operator in the GW framework.[48] The relative values are also summarized in Table I.

It should be pointed out that band gaps calculated at the *electronic* level are comparable with the values obtained

TABLE I. Band gaps calculated at the LDA level $E_{g-\text{LDA}}$, and at the GW level E_{g-GW}, the excitation energy (E^I) and binding energy (E_b) of the first bright exciton (I^1), and the location of the lowest-energy dark excitons (E^D). Indirect band-gap values of g-CN2 are shown in parentheses. All values are in eV.

	$E_{g-\text{LDA}}$	E_{g-GW}	E^I	E_b	E^D
g-C_3N_4	1.32	3.35	3.79	1.20	2.47
g-CN1	1.43	4.24	3.58	2.52	2.43
g-CN2	2.09 (1.11)	5.22 (4.15)	3.90	1.32	2.21

from experimental photoemission and inverse-photoemission spectroscopy instead of absorption spectra. This is because the e-h Coulomb attraction involved in optical excitations is not considered in the calculation of single-particle spectra. As a consequence, it is inappropriate to verify the calculated electronic band gap with the *optical* gap extrapolated from the absorption spectrum as a reference, as done in Ref. 23. The difference between electronic and optical gaps can be attributed to the binding energy of bound excitons, as discussed later.

The optical absorption spectra, which are directly associated with the imaginary part of the macroscopic dielectric function ε_M, were calculated for g-CNs at the DFT-RPA level. Further, we also studied modifications to the dielectric response introduced by the so-called crystal local field effects (LFE). With LFE included, the microscopic part of the density variation of the Hartree potential corresponds to considering the off-diagonal elements in the matrix inversion $\varepsilon \rightarrow \varepsilon^{-1}$.[35,49] Without considering these effects, only the independent-particle transitions are involved and inhomogeneities in the dielectric response are neglected completely.[50] In other words, this approach is equivalent to applying Fermi's golden rule. For light polarization parallel to the g-CNs surface plane, as shown in Figs. 2(c) and 2(d), LFE only cause slight modifications to the spectral profile. For light polarization perpendicular to the surface plane, however, LFE cause distinct intensity suppression. This results in the dramatic optical anisotropy and renders g-CNs almost optically transparent for light polarization perpendicular to the surface plane. As a consequence, LFE are the most important ingredient in order to explain this depolarization effect, which can result in a considerably small polarizability for light polarization perpendicular to the surface plane. Consequently, shortcomings in calculations are often not due to the quality of the band structure calculation itself, but the neglect of microscopic electric fields stemming from the bound surface charges in response to the external field.[51]

The optical absorption spectra of g-CN1 and g-CN2 calculated with (GW + BSE) and without (GW + RPA) e-h interaction are shown in Figs. 3 and 4, respectively. Due to the weak absorption strength for light polarization perpendicular to the surface plane, here we only present the optical spectra for parallel-polarized light. The optical spectrum at the GW + RPA level demonstrates that the direct optical transitions are significantly blue-shifted compared to those at the DFT-RPA level. This is because of the QP corrections on top of the GW approximation. In addition, inclusion of $e-e$ correlation also has slight influence on the spectral profile calculated within independent-particle approximations. As shown in Figs. 3 and 4, dramatic changes occur when e-h Coulomb interactions

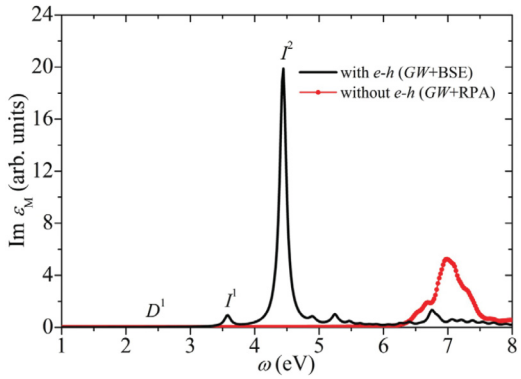

FIG. 3. (Color online) Imaginary part of the macroscopic dielectric function ε_M for light polarization parallel to the g-CN1 surface plane calculated with (black line) and without (red dot line) consideration of the e–h interactions, i.e., GW + BSE and GW + RPA, respectively. Five occupied and ten empty bands are included when calculating the optical absorption spectrum at the GW + BSE level. A Lorentzian broadening of 0.1 eV was adopted.

are included in the calculation: Optical absorptions of g-CNs are greatly modified and strongly bound exciton states well below the onset of single-particle transition continuum are indicated. This prominent variation from the single-particle spectrum reveals a weight redistribution of the oscillator strength, most of which is collected by the strongly bound excitonic states. There is an obvious cancellation effect between the band-gap opening due to the QP corrections and the redshift of optical absorption due to the excitonic effects. For both g-CN1 and g-CN2 systems, we conclude that strong excitonic effects dominate the optical absorption properties.

For g-CN1, as shown in Fig. 3, the first optically active (bright) exciton emerges at 3.58 eV (I^1), and the second one at 4.44 eV (I^2). The first exciton in g-CN1 is in the nature of multiband transitions from the top of the valence band, which is doubly degenerated, to the third conduction band at the Γ point, as shown in Fig. 2(a). For light polarization parallel to the surface plane, g-CN1 shows no transition from the top of the valence band to the bottom of the conduction band at the Γ point as this process is forbidden by band symmetry. I^2 is mainly contributed by the transitions from the last valence band to the first conduction band at k points halfway between the Γ and M points [see Fig. 2(a)]. The binding energies of I^1 and I^2 in g-CN1 are 2.52 and 1.65 eV, respectively. Such large binding energies are due to the quantum confinement and the less efficient screening. For g-CN1, there are also many optically inactive (dark) excitons distributed below and among the bright excitons, with the lowest one (D^1) located at 2.43 eV. The dark states are dipole forbidden and thus provide a competing path for nonradiative decay of optical excitations, which can affect the luminescence yield.

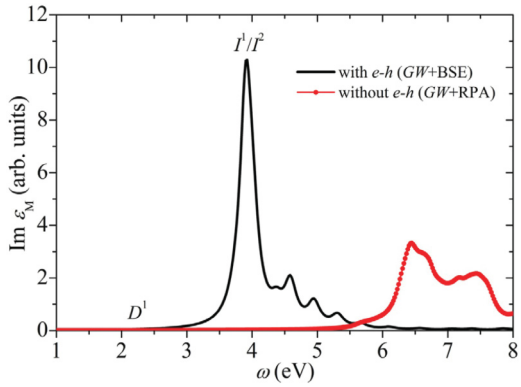

FIG. 4. (Color online) Imaginary part of the macroscopic dielectric function ε_M for light polarization parallel to the g-CN2 surface plane calculated with (black line) and without (red dot line) consideration of the e-h interactions, i.e., GW + BSE and GW + RPA, respectively. Five occupied and ten empty bands are included when calculating the optical absorption spectrum at the GW + BSE level. A Lorentzian broadening of 0.1 eV was adopted.

In the case of g-CN2, the first optically active exciton I^1, which is doubly degenerated with I^2, locates at 3.90 eV. I^1/I^2 is dominantly composed of transitions between a single pair of quasiparticle bands, i.e., as shown in Fig. 2(b), the last valence band and the first conduction band at the k points one-third of the way from the K to the Γ point, with a large binding energy of 1.32 eV. There are also many dark excitons distributed in energy below the bright excitons, with the lowest one, D^1, located at 2.21 eV, as shown in Fig. 4.

Such large excitonic effects have also been theoretically predicted in hexagonal SiC and BN monolayer structures,[52,53] which present a similar two-dimensional confinement with anisotropic and reduced screening as g-CNs. The inclusion of excitonic effects, which are missing in GW + RPA spectra, is crucial for the quantitative and qualitative description of the optical properties. As shown above, for fully condensed and infinite g-CN networks, excitonic effects are responsible for the optical absorption properties. Compared with the resonant excitons, such as those in graphene,[24–26] bound excitons are of particular interest due to their well-defined binding energies and longer lifetimes and thus hold the promise for applications in optoelectrics and electronics.

In order to explicitly represent the correlation between excited electrons and holes, the Bethe-Salpeter two-particle's Hamiltonian was diagonalized to obtain the wave functions of excitons. In Fig. 5, electron probability distributions

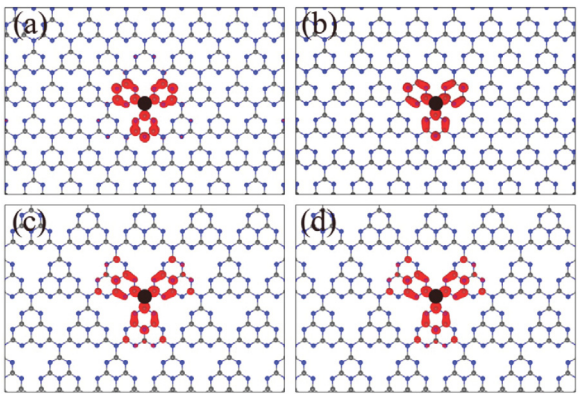

FIG. 5. (Color online) Three-dimensional electron probability distributions $|\psi(\mathbf{r}_e;\mathbf{r}_h)|^2$ in real space as a function of electron position with the hole position (black dot) fixed slightly above a N atom for the excitonic states I^1 and I^2 of g-CN1 [(a) and (b)], and of g-CN2 [(c) and (d)].

$|\psi(\mathbf{r}_e;\mathbf{r}_h)|^2$ for the bound excitons I^1 and I^2 of g-CNs (Figs. 3 and 4) are shown as a function of the electron position $\mathbf{r}_e$ with the hole position $\mathbf{r}_h$ fixed slightly above a N atom. $|\psi(\mathbf{r}_e;\mathbf{r}_h)|^2$ describes how the quasielectrons and quasiholes in excited states are correlated in real space. As indicated in Fig. 5, all of the wave functions of the bound excitons resemble threefold symmetry and indicate relatively small distribution radii. The excited electrons are delocalized on the C and N atoms surrounding the hole, which reflects the hybridization character of the conduction band. Here, we clearly see the huge overlap and thus the weak electronic screening between e-h wave functions, which manifests the strong binding of the excitons in g-CNs.

As discussed above, strong excitonic effects dominate the optical response of fully condensed g-CN networks with the formation of strongly bound excitons. Many-body effects are in close relation with the quantum confinement, or the dimensionality of the structure. In order to confirm this conclusion, we also studied the many-body effects in quasi-two-dimensional g-C_3N_4 in bulk phase with a layer distance of 4.05 Å [see Fig. 6(a)]. As shown in Table I, the band gap, the excitation energy, and the binding energy of the first bright exciton (I^1), and the location of the lowest-energy dark state (D^1) are 1.32, 3.35, 3.79, 2.52, and 2.43 eV, respectively. From the values, we note an increase of 0.11 eV in the band gap of g-CN1 compared with that of g-C_3N_4 in bulk phase, which can be attributed to the stronger confinement effect in the former. In addition, the QP correction to the electronic gap of g-CN1, 2.81 eV, is obviously larger than that to bulk g-C_3N_4, 2.03 eV, which is due to the enhanced e-e correlation in two-dimensional g-CN1. Absorption spectra calculated with and without the inclusion of e–h attractive interactions [Fig. 6(b)] as well as the electron probability distributions $|\psi(\mathbf{r}_e;\mathbf{r}_h)|^2$ of the bright excitons I^1 and I^2 [Figs. 6(c) and 6(d)] of g-C_3N_4 in bulk phase are presented. The excitation energy of the first bright exciton, 3.58 eV in two-dimensional g-CN1, is 0.21 eV lower than that in three-dimensional bulk g-C_3N_4 of 3.79 eV.

A similar trend in the DFT-calculated band gap was also indicated in the work of Wang *et al.*:[14] The band gap of the melem molecule is 3.5 eV, and the band gaps of the infinite g-C_3N_4 sheet and polymeric melon are 2.1 and 2.6 eV, respectively. It means that the band gap increases as the dimensionality of the system decreases. An increase of 0.5 eV in the band gap can be noticed when going from the two-dimensional monolayer structure to the one-dimensional chain structure of g-C_3N_4 (it is actually not a stoichiometric C_3N_4 in Ref. 14). In Ref. 14, H_2 evolution was realized upon polymeric g-C_3N_4, for which is suggested an optical gap of 2.7 eV. In polymeric structures with stronger quantum confinement compared to bulk and infinite g-C_3N_4 single layers, optical properties are also expected to be influenced by strong excitonic effects. As argued above, the optical gap of polymeric g-C_3N_4 of 2.7 eV probably can be considered as the onset of excitonic absorption. The relatively small difference of 0.1 eV between the electronic and optical band gap is an indication of the cancellation effect addressed

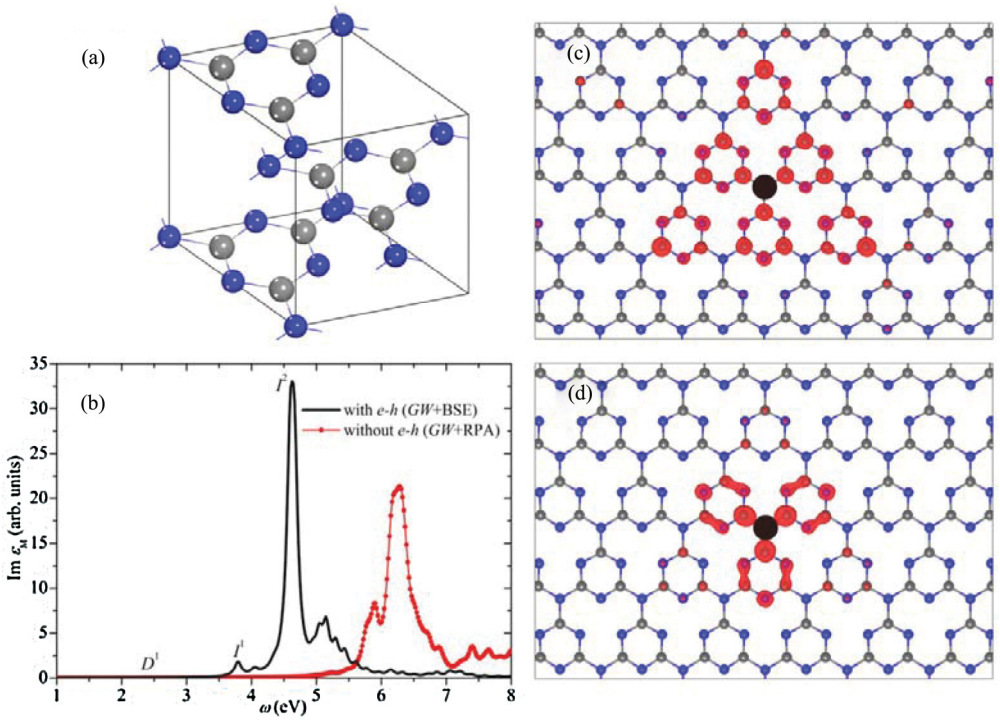

FIG. 6. (Color online) g-C_3N_4 structure in bulk phase (a); gray and blue spheres represent C and N atoms, respectively. Imaginary part of the macroscopic dielectric function ε_M for light polarization parallel to the g-C_3N_4 layer calculated with (black line) and without (red dot line) consideration of the e-h interactions, i.e., GW + BSE and GW + RPA, respectively (b); five occupied and ten empty bands are included when calculating the optical absorption spectra at the GW + BSE level; a Lorentzian broadening of 0.1 eV was adopted. Three-dimensional electron probability distributions $|\psi(\mathbf{r}_e;\mathbf{r}_h)|^2$ in real space for the excitonic states I^1 (c) and I^2 (d) of g-C_3N_4 in the bulk phase. The hole position (black dot) had been fixed slightly above a N atom.

in this work. On the other hand, our results suggest that a *tunable* band gap probably can be realized to some extent by adjusting the condensation (dimensionality) of g-C_3N_4 to initiate absorption in the visible light region to improve solar energy conversion efficiency.

IV. CONCLUSIONS

In conclusion, results concerning the electronic and optical properties of g-C_3N_4 are presented by means of the many-body Green's function method. In order to obtain the quantitative band gaps, QP self-energy corrections to DFT eigenvalues are calculated within the GW approximation. An electronic band gap of 4.24 eV is determined for the g-C_3N_4 monolayer structure constructed from triazine, while 5.22 eV (direct) and 4.15 eV (indirect) are determined for the g-C_3N_4 monolayer structure based on tri-s-triazine. Such significant QP corrections are an indication of the enhanced e-e correlation in systems with low dimensionality. It is important to include LFE to explain the depolarization effect in optical response to light polarization perpendicular to the surface plane. By solving the BSE on top of GW approximation, optical absorption spectra of g-C_3N_4 are obtained with e-h attractive interaction included. With the formation of strong bound excitons well below the onset of the single-particle transition continuum, optical spectra of g-C_3N_4 are dominated by strong excitonic effects. Binding energies of the first bright exciton are 2.52 and 1.32 eV for g-CN1 and g-CN2, respectively. The absorption can be redshifted to the visible light region by tuning the dimensionality, making g-G_3N_4 a visible light-driven photocatalyst. On the other hand, well-defined binding energies and long lifetimes of the excitons make g-C_3N_4 also a potential candidate for optoelectric and electronic devices.

ACKNOWLEDGMENTS

W.W. thanks Z. Meng, H. Pan, C. Sun, Y. Ma, and J. Zhang for the useful discussion on the g-CNs structure. The authors gratefully acknowledge support from the European Union through the Marie-Curie Initial Training Network ELCAT, Proposal No. 214936-2, 2008–2012 and the ERC-Starting Grant THEOFUN. Support by the BMBF (Bundensministerium für Bildung und Forschung) through the network H_2-NanoSolar is also acknowledged.

*timo.jacob@uni-ulm.de

[1] A. Y. Liu and M. L. Cohen, Science **245**, 841 (1989).
[2] L. W. Yin, Y. Bando, M. S. Li, Y. X. Liu, and Y. X. Qi, Adv. Mater. **15**, 1840 (2003).
[3] M. H. V. Huynh, M. A. Hiskey, J. G. Archuleta, and E. L. Roemer, Angew. Chem., Int. Ed. **43**, 5658 (2004); **44**, 737 (2005).
[4] D. R. Miller, D. C. Swenson, and E. G. Gillan, J. Am. Chem. Soc. **126**, 5372 (2004).
[5] Y. J. Zhang, A. Thomas, M. Antonietti, and X. C. Wang, J. Am. Chem. Soc. **131**, 50 (2009).
[6] G. Liu, P. Niu, C. H. Sun, S. C. Smith, Z. G. Chen, G. Q. Lu, and H.-H. Cheng, J. Am. Chem. Soc. **132**, 11642 (2010).
[7] B. Jurgens, E. Irran, J. Senker, P. Kroll, H. Muller, and W. Schnick, J. Am. Chem. Soc. **125**, 10288 (2003).
[8] J. R. Holst and E. G. Gillan, J. Am. Chem. Soc. **130**, 7373 (2004).
[9] E. Kroke, M. Schwarz, E. Horath-Bordon, P. Kroll, B. Noll, and A. D. Norman, New J. Chem. **26**, 508 (2002).
[10] M. Groenewolt and M. Antonietti, Adv. Mater. **17**, 1789 (2005).
[11] A. Vinu, K. Ariga, T. Mori, T. Nakanishi, S. Hishita, D. Golberg, and Y. Bando, Adv. Mater. **17**, 1648 (2005).
[12] S. Stankovich, D. A. Dikin, G. H. B. Dommett, K. M. Kohlhaas, E. J. Zimney, E. A. Stach, R. D. Piner, S. T. Nguyen, and R. S. Ruoff, Nature (London) **442**, 282 (2006).
[13] D. A. Dikin, S. Stankovich, E. J. Zimney, R. D. Piner, G. H. B. Dommett, G. Evmenenko, S. T. Nguyen, and R. S. Ruoff, Nature (London) **442**, 457 (2006).
[14] X. C. Wang, K. Maeda, A. Thomas, K. Takanabe, G. Xin, J. M. Carlsson, K. Domen, and M. Antonietti, Nat. Mater. **8**, 76 (2009).
[15] X. C. Wang, X. F. Chen, A. Thomas, X. Z. Fu, and M. Antonietti, Adv. Mater. **21**, 1609 (2009).
[16] X. C. Wang, K. Maeda, X. F. Chen, K. Takanabe, K. Domen, Y. D. Hou, X. Z. Fu, and M. Antonietti, J. Am. Chem. Soc. **131**, 1680 (2009).
[17] J. S. Zhang, X. F. Chen, K. Takanabe, K. Maeda, K. Domen, J. D. Epping, X. Z. Fu, M. Antonietti, and X. C. Wang, Angew. Chem., Int. Ed. **49**, 441 (2010).
[18] Y. Wang, J. S. Zhang, X. C. Wang, M. Antonietti, and H. R. Li, Angew. Chem., Int. Ed. **49**, 3356 (2010).
[19] Y. J. Zhang, T. Mori, J. H. Ye, and M. Antonietti, J. Am. Chem. Soc. **132**, 6294 (2010).
[20] Y. J. Zhang, T. Mori, L. Niu, and J. H. Ye, Energy Environ. Sci. **4**, 4517 (2011).
[21] J. S. Lee, X. Q. Wang, H. M. Luo, and S. Dai, Adv. Mater. **22**, 1004 (2010).
[22] A. J. Du, S. Sanvito, and S. C. Smith, Phys. Rev. Lett. **108**, 197207 (2012).
[23] A. J. Du, S. Sanvito, Z. Li, D. W. Wang, Y. Jiao, T. Liao, Q. Sun, Y. H. Ng, Z. H. Zhu, R. Amal, and S. C. Smith, J. Am. Chem. Soc. **134**, 4393 (2012).
[24] L. Yang, Nano Lett. **11**, 3844 (2011).
[25] P. Cudazzo, C. Attaccalite, I. V. Tokatly, and A. Rubio, Phys. Rev. Lett. **104**, 226804 (2010).
[26] L. Yang, J. Deslippe, C.-H. Park, M. L. Cohen, and S. G. Louie, Phys. Rev. Lett. **103**, 186802 (2009).
[27] P. E. Trevisanutto, M. Holzmann, M. Côté, and V. Olevano, Phys. Rev. B **81**, 121405 (2010).
[28] L. Yang, M. L. Cohen, and S. G. Louie, Nano Lett. **7**, 3112 (2007).
[29] W. Wei and T. Jacob, Phys. Rev. B **86**, 165444 (2012).
[30] G. Onida, L. Reining, and A. Rubio, Rev. Mod. Phys. **74**, 601 (2002).
[31] M. Rohlfing and S. G. Louie, Phys. Rev. B **62**, 4927 (2000).

[32]G. F. Luo, X. M. Qian, H. B. Liu, R. Qin, J. Zhou, L. Z. Li, Z. X. Gao, E. G. Wang, W.-N. Mei, J. Lu, Y. L. Li, and S. Nagase, Phys. Rev. B **84**, 075439 (2011).
[33]A. Marini and R. Del Sole, Phys. Rev. Lett. **91**, 176402 (2003).
[34]M. Bruno, M. Palummo, A. Marini, R. Del Sole, and S. Ossicini, Phys. Rev. Lett. **98**, 036807 (2007).
[35]M. Bruno, M. Palummo, A. Marini, R. Del Sole, V. Olevano, A. N. Kholod, and S. Ossicini, Phys. Rev. B **72**, 153310 (2005).
[36]D. Prezzi, D. Varsano, A. Ruini, A. Marini, and E. Molinari, Phys. Status Solidi B **244**, 4124 (2007).
[37]L. Wirtz, A. Marini, and A. Rubio, Phys. Rev. Lett. **96**, 126104 (2006).
[38]M. Bockstedte, A. Marini, O. Pankratov, and A. Rubio, Phys. Rev. Lett. **105**, 026401, (2001).
[39]P. Giannozzi *et al.*, J. Phys.: Condens. Matter **21**, 395502 (2009).
[40]A. Marini, C. Hogan, M. Grüning, and D. Varsano, Comput. Phys. Commun. **180**, 1392 (2009).
[41]R. W. Godby and R. J. Needs, Phys. Rev. Lett. **62**, 1169 (1989).
[42]R. Ahuja, S. Auluck, J. M. Wills, M. Alouani, B. Johansson, and O. Eriksson, Phys. Rev. B **55**, 4999 (1997).
[43]A. L. Fetter and J. D. Walecka, in *Quantum Theory of Many-Particle Systems* (Dover, New York, 2003), Chap. 15, p. 565.
[44]C. A. Rozzi, D. Varsano, A. Marini, E. K. U. Gross, and A. Rubio, Phys. Rev. B **73**, 205119 (2006).
[45]M. Shishkin, M. Marsman, and G. Kresse, Phys. Rev. Lett. **99**, 246403 (2007).
[46]M. van Schilfgaarde, T. Kotani, and S. Faleev, Phys. Rev. Lett. **96**, 226402 (2006).
[47]M. Deifallah, P. F. McMillan, and F. J. Corà, Phys. Chem. C **112**, 5447 (2008).
[48]D. Prezzi, D. Varsano, A. Ruini, A. Marini, and E. Molinari, Phys. Rev. B **77**, 041404 (2011).
[49]A. G. Marinopoulos, L. Reining, A. Rubio, and N. Vast, Phys. Rev. Lett. **91**, 046402 (2003).
[50]J. G. Vilhena, S. Botti, and M. A. L. Marques, Appl. Phys. Lett. **96**, 123106 (2010).
[51]A. G. Marinopoulos, L. Wirtz, A. Marini, V. Olevano, A. Rubio, and L. Reining, Appl. Phys. A **78**, 1157 (2004).
[52]H. C. Hsueh, G. Y. Guo, and S. G. Louie, Phys. Rev. B **84**, 085404 (2011).
[53]B. Arnaud, S. Lebègue, P. Rabiller, and M. Alouani, Phys. Rev. Lett. **96**, 026402 (2006).